CRYO/99/013
February 20, 1999

Stability and Protection of CICC's - An Updated Designer's View

L. Bottura

Distribution: Internal

Published: Cryogenics, **38**, 491-502, 1998

Summary

This paper gives un update on stability and protection of CICC's, with a main focus on simple analytical formulae to be used for cable design purposes. The status of the present understanding is reviewed, collecting the main results as far as possible into a consistent notation. Various additional aspects of present interest are briefly discussed, such as special cable configurations (hybrid cables, cables with additional cooling channels) and operation in superfluid helium. Some considerations on cable current distributions, and its effect on cable stability, are given

1. Introduction

Stability and protection are two fundamental aspects of the physics of superconducting cables that have deserved much attention since the first practical application of superconductors in magnets[1]. Both are still of major concern for today's designer: cable stability is one of the factors determining the reliability and availability of the magnetic system, while protection in case of quench is of paramount importance in magnetic systems of large stored energy. The natural outcome of this concern is the effort towards the definition of a *design code* that gives an optimised cable design, satisfying stability and protection constraints. Some examples of how this has been translated into practice for force-flow cooled, cable-in-conduit conductors (CICC's) can be found in Refs. [2-4]. Simple analytical models of the stability margin and quench evolution were used there to deduce the cable design with the maximum operating cable space current density, i.e. the minimum cable cross section for a given operating current. In the meanwhile understanding of both processes has improved, and new conductor operating conditions (superfluid helium) and layouts (hybrid cables with co-wound stabilizer, parallel cooling channel) are considered. This paper starts with a summary of design procedures commonly used for stability and protection of CICC's and already reviewed in Ref. [4]. The aim is then to update these results based on the latest evolution of knowledge and designs. All symbols used are collected in Table 1 for clarity. In addition most of them are coherent with the notation of Ref. [4].

2. Stability

2.1 Limiting current and helium heat sink

We wish as the first step to design the CICC that will operate at maximum current density withstanding a given energy deposition over a given duration and length. This last is indeed nothing else but the definition of the energy margin ΔE of the cable. Usually, for reasons of safety margins and simplicity, the energy input is assumed to take place over a long (infinite) length and a short (infinitesimal) time duration. This is representative, for instance, of the energy deposition through AC loss caused by electromagnetic transients such as plasma disruption in a fusion experiment. In reality the perturbation spectrum covers a wide scale of lengths and times, a fact that must not be forgotten in the detailed analysis of the cable stability. However, the choice of a long lenth and a short time is a *worst case* and therefore appropriate for design purposes.

The basic tools for the design of a stable CICC are the two concepts of the limiting current and of the heat sink provided by the helium. In the original ideas developed by Dresner [5] the stability margin of a CICC is approximately equal to the total heat sink for operation below a *limiting current*, a regime also called *well-cooled* after Schultz and Minervini [6]:

$$\Delta E \approx \Delta E_{\max} \tag{1}$$

where ΔE_{max} is the maximum heat sink between the operating and current sharing temperatures:

$$\Delta E_{\max} = \int_{T_{op}}^{T_{cs}} \frac{f_{stab} C_{stab} + f_{SC} C_{SC} + f_{he} C_{he}}{\left(f_{stab} + f_{SC}\right)} dT \tag{2}.$$

Above the limiting current, in the *ill-cooled* regime, the stability margin is of the order of the strands heat capacity plus the energy transferred to the helium during the heat pulse τ_e and the recovery time τ_r [7]:

$$\Delta E \approx \int_{T_{op}}^{T_{cs}} \frac{f_{stab} C_{stab} + f_{SC} C_{SC}}{\left(f_{stab} + f_{SC}\right)} dT + \frac{4K_p}{d}\left(T_{cs} - T_{op}\right)\int_0^{\tau_e+\tau_r} h dt \tag{3}$$

where we note for completeness that the second integral above is usually small (negligible in our assumption of instantaneous energy deposition). The definition of the limiting current is a direct consequence of the balance of Joule heat generation and heat removal, obtained after Stekly [8] as:

$$I_{\lim} = \sqrt{\frac{A_{stab} p_w h\left(T_c - T_{op}\right)}{\rho_{stab}}} \tag{4}$$

or, using the material fractions in the cable to obtain an expression of the cable space current density [4]:

$$J_{op} = \cos(\theta)\sqrt{f_{stab}\left(f_{stab} + f_{SC}\right)\frac{4K_p h\left(T_c - T_{op}\right)}{\rho_{stab} d}} \tag{5}.$$

The power balance implied by Eq. (4) expresses a condition for recovery, and is referred to the end of the heat pulse. In the interpretation of Dresner[5] and Schultz and Minervini[6] below I_{lim} the full heat sink of the cable can be used because the strands can recover from an arbitrary temperature excursion, while above I_{lim} recovery is conditional. Hence the heat sink provided by the helium is efficiently used only in the well-cooled regime, which is therefore characterized by an energy margin much larger than in the ill-cooled regime. This ideal situation has been schematically represented in Fig. 1. The sharp rise in stability margin located at the limiting current is obviously the optimal design point because at the limiting current the best possible use is made of the helium available. The cable is designed fixing a tentative value of the material fractions and using Eq. (2) to determine the T_{cs} that provides the necessary heat sink. A value of T_{cs} corresponds to an operating current density in the superconductor and thus, at fixed material fractions, in the cable space. This current density must be matched to the limiting current density of Eq. (5). Scanning the range of *feasible* material fractions the optimum selection can be found.

The main unknown of this procedure is the value of the heat transfer coefficient *h*. As discussed by Dresner [5] the heating induced flow in helium affects the formation and evolution of the boundary layer. The determination of *h* becomes in principle coupled with the external and Joule heat input. The approach proposed in [5] and [9] is to use a scaling law empirically fitted to data. The limitation of this method is that an extrapolation becomes risky in the regions where we lack experimental data on the cable configuration. A less rigorous approach is to design using a value of *h* directly derived from a data base of experiments. Typical values for *h* over a wide range of cables and operating conditions have been compiled by Lue [10]. They range from 400 W/m^2 K to 1400 W/m^2 K, with an average of the order of 1000 W/m^2 K.

The simple procedure outlined above is very useful for design and optimisation. It is however much simplified and should be used with caution. In particular this model makes two basic assumptions that we wish to challenge:

- the recovery condition Eq. (4), originally developed for bath cooled magnets, implicitly states that the helium temperature has not changed during the transient;
- the cable properties are assumed to be homogeneous, and in particular the current distribution is taken uniform in the cable cross section.

The assumption of constant helium temperature can be waved at the cost of little additional complication as shown in the next section. Current distribution in pulsed field experiments has been proven to have a serious impact on the cable stability and its current carrying capacity. Here we will address current distribution effects only from the point of view of the influence on the energy balance in the cable cross section.

2.2 Helium bath temperature changes

The amount of helium present in the cable space of a CICC is limited, and any energy deposition will cause the *bath* temperature to increase. During the thermal transient the helium and strand temperatures will follow complex trajectories, but in case of recovery we know that the end condition is of equal temperatures, both below T_{cs}. We call this final value the *recovery* temperature T_{rec} [11].

As stated previously, the recovery condition implied by the power balance of Joule heat production and heat removal used to derive Eq. (4) must hold at the end of the thermal transient. At this time the helium temperature is already approximately T_{rec} because little extra energy flows into the heat sink during the last phase of the recovery. Hence the power balance to be satisfied for recovery to take place is the following:

$$\frac{\rho_{stab} I_{op}^2}{A_{stab}} \le p_w h\left(T_c - T_{rec}\right) \tag{6}$$

which evidences the fact that heat transfer at the strand surface takes place under a reduced temperature difference. This gives the following value for T_{rec}:

$$T_{rec} = T_c - \frac{\rho_{stab} I_{op}^2}{p_w h A_{stab}} \tag{7}.$$

As evident from Eq. (7), the recovery temperature varies as a function of the operating current. In fact at the limiting current given by Eq. (4) we have that $T_{rec}=T_{op}$ which demonstrates that the helium is not allowed to absorb any significant heat otherwise the power balance cannot be satisfied. At currents below I_{lim} a smaller temperature difference is necessary to satisfy the power balance condition and T_{rec} increases above T_{op}, thus giving room for using the helium heat sink during the transient. Optimal usage of the helium heat sink is obtained when the recovery takes place even in case of helium temperature increase up to T_{cs}, the maximum possible value. This condition, which we can express as $T_{rec}=T_{cs}$, can be conveniently translated into a definition of a *lower limiting current*:

$$I_{\lim}^{low} = \frac{A_{stab}\, p_w h\left(T_c - T_{op}\right)}{\rho_{stab} I_c} \tag{8}.$$

We stress that the full heat sink in the cable cross section ΔE_{max} is completely used only at a current equal or below $I_{\lim}^{low}$. A transition takes place between $I_{\lim}^{low}$ and I_{lim}, where the energy margin decreases gradually from the maximum value ΔE_{max} to the ill-cooled value given by Eq. (3). In the transition regime ΔE decreases proportionally to the square of the operating current, as shown in [11]. Figure 1 shows a comparison of this behaviour to the simpler well-cooled/ill-cooled model discussed in the previous section.

The interest for the designer is that the value of the lower limiting current and of the energy margin in the transition region can be expressed using the cable fractions and the cable space operating current density. After [4] and [11] we write that the cable space operating current density at the lower limiting current is:

$$J_{op} = \cos(\theta)\frac{4K_p h}{\rho_{stab} d}\frac{\left(T_c - T_{op}\right)}{J_c}\frac{f_{stab}}{f_{SC}}\left(f_{stab} + f_{SC}\right) \tag{9}$$

As demonstrated in [11], if we take into account the energy margin transition between $I_{\lim}^{low}$ and I_{lim} the cable design with maximum cable space current density is obtained operating exactly at the lower limiting current. This can be intuitively understood as a consequence of the fact that below $I_{\lim}^{low}$ we have an excess of stabilizer compared to the one necessary to use the maximum heat sink, while above $I_{\lim}^{low}$ the stability margin is lower than the maximum available, and the helium inventory is not properly used for stabilization. In summary, Eq.(9) should be used in the place of Eq. (5) of the previous section. A cable designed using Eq. (9) will have more copper than the one obtained from Eq. (5), but will also take into proper account the recovery condition, thus requiring no safety factor.

A final result of this analysis is that we can derive a limit for the maximum useful ratio of stabilizer to superconductor in the strand. This maximum ratio is reached when the lower limiting current is equal to the operating current corresponding to the minimum requested temperature margin $\Delta T=T_{cs}-T_{op}$. Using Eq. (9) we can write this condition as:

$$\left.\frac{f_{stab}}{f_{SC}}\right|^{\max} = \frac{1}{2}\left[\sqrt{1+\frac{\rho_{stab} d J_c^2}{\cos(\theta) K_p h\left(T_c - T_{op}\right)}\left(1-\frac{\Delta T}{\left(T_c - T_{op}\right)}\right)} - 1\right] \qquad (10).$$

Adding stabilizer above the ratio given by Eq. (10) will have the detrimental effect of reducing the superconductor fraction and necessarily the operating current density in order to maintain the specified temperature margin. As an example the limit above is of the order of 2 for a Nb3Sn strand in a 12 T field with a temperature margin of 2 K, a value which is in any case above the typical manufacturing range. For a NbTi strand, operated in a 7 T field with the same temperature margin, the typical maximum useful copper:NbTi ratio is about 5.

2.3 Current distribution effects

Current distribution is not necessarily, possibly never, uniform in a superconducting cable. A current imbalance can have several origins, such as a difference in the series resistance in the cable (joints or high field behaviour of the strands), or a difference in the inductive voltages on the strands during ramping (field variations along the cable length or transposition errors). We can describe the current distribution using the density of strands $\alpha(i)$ carrying a normalized current $i=I/I_c$, a function defined such that its zero-th order moment with respect to i is the number of strands and the first moment is the average normalised current carried by the cable $i_{op}= I_{op}/I_c$. The density function must necessarily be zero at the critical current. In fact α is zero for any $i > i_{max}$, the normalised current carried by the most *overloaded* strand.

The first and obvious effect of a non-uniform current distribution is that the strands carrying a current above i_{op} have less margin, compared to the average, and thus are more prone to quenching. During a thermal transient these strands are the first to start Joule heating, while a current transfer process takes place with a characteristic time τ_i. We can identify two limiting conditions determined by the comparison of the current transfer time scale τ_i and the recovery time scale τ_r. In the case $\tau_i >> \tau_r$ the normal strands can produce Joule heat for a very long time, eventually driving the whole cable normal. In the opposite case, when $\tau_r >> \tau_i$, the current transfer can be considered instantaneous and the cable acts as if it had a uniform current distribution. In practice in the first case, $\tau_i >> \tau_r$, the cable energy margin is equal to

the energy margin of the strand that is carrying the largest current $\Delta E(i_{max})$, while in the opposite case the energy margin is the same as for a cable with uniform current density, i.e. $\Delta E(i_{op})$. These two limiting cases provide minimum and maximum bounds for the cable energy margin. A non uniform current distribution and a finite current transfer time always result in an energy margin below the maximum value, because of the increased Joule heating produced during the current transfer process. The actual location of the energy margin between the two bounds depends on the details of the current distribution (the function α), and on the current transfer and recovery process.

This situation has been sketched in Fig. 2, where we show an hypothetical current distribution function $\alpha(i)$ and the corresponding upper and lower bound for the energy margin. At a given operating fraction i_{op} the energy margin (dashed line) must be between the upper bound given by the *collective* energy margin and the lower bound given by the *worst strand* energy margin. As shown there, the lower bound is obtained from the collective energy margin by a shift of i_{max}-i_{op} in the current fraction. Note that this shift is not necessarily a constant throughout the operating current range, but can vary as a function of time and current. A behaviour similar to the one depicted in Fig. 2 was indeed observed experimentally[11a] on a CICC with formvar insulated NbTi strands used in the Demonstration Poloidal Coil DPC-U1. The energy margin reported there was different by one order of magnitude depending on whether the stability test was performed before or after a sequence of short heating pulses, and the difference was attributed to the fact that a limited normalcy can contribute to a better current distribution among strands.

As we stated previously, the current distribution is generally not known in a CICC. Hence the design must be made tolerant to an arbitrary current distribution through the capability to redistribute the current excess from overloaded strands. To demonstrate that this is possible we must first derive an estimate of the time scales τ_r and τ_i. A good approximation of the characteristic recovery time is given by the time constant of the temperature difference between strands and helium:

$$\tau_r \approx \frac{f_{stab}C_{stab} + f_{SC}C_{SC}}{4K_p h\left(f_{stab} + f_{SC}\right)} d\,. \tag{11}$$

and for a typical CICC we have that $\tau_r \approx 1.5$ ms. The current transfer time is determined by the geometry of the cable as well as by the transverse and longitudinal resistances. An estimate of the current transfer time from a quenched length L_q is [12]:

$$\tau_i \approx \begin{cases} \left(\frac{L_i}{L_q}\right)^2 \frac{2L' - 2M'}{\pi R'} & L_q << L_i \\ \frac{2L' - 2M'}{\pi R'} & L_i << L_q \end{cases} \tag{12}$$

where L' and M' are the self and mutual inductance per unit length of the strands, R' is the strand resistance per unit length. The current transfer length L_i is given by:

$$L_i = \frac{1}{\sqrt{R'G'}} \tag{13}$$

where we introduced the interstrand conductance per unit length *G'*. Following our previous discussion we must make the current transfer time as small as possible so that the energy margin approaches the *collective*, uniform current density limit. After Eq. (12) this corresponds to a negligible current transfer length compared to the quenched length. The only free parameter in Eq. (13) is the interstrand conductance, which we need therefore to make as large as possible compatibly with the requirement of low losses. In fact, we can use Eq. (13) to compute the minimum value necessary to design a CICC with the fastest current redistribution:

$$G' \geq \frac{1}{L_q^2 R'} \tag{14}.$$

If we take typical values for the self and mutual inductance and longitudinal resistance of a 1 mm thick, copper stabilized strand in a large CICC bundle ($2(L'-M') \approx 1$ μH/m, $R' \approx 2$ mΩ/m), and we take an estimate of the minimum conceivable normal length $L_q \approx 15$ cm, of the order of the minimum propagating zone (MPZ) for a large size CICC, we obtain that the minimum value of the interstrand conductance per unit length is of the order of 30,000 Ω^{-1}/m. Typical values obtained in CICC cabled with coated strands range widely, also because of the random definition of the number and geometry of the interstrand contacts. Values measured by Takayasu [13] on Cr coated Nb3Sn strands are of the order of 100,000 Ω^{-1}/m and seem to provide a bottom estimate, indicating that a CICC can indeed fulfill the condition Eq. (14) on the current transfer length when the strands are not insulated. The current transfer time is then given by the second of Eq. (12), i.e. with the choice of parameters above $\tau_i \approx 0.5$ ms. We see that τ_i and τ_r are of the same order, indeed making the estimate of the cable energy margin a difficult task. However both values are small, so that in the energy balance we can neglect the Joule heat produced during the current transfer and recovery phases when compared to the heat sink available. Therefore for a single event the energy margin of the cable is close to the ideal homogeneous value $\Delta E(i_{op})$ discussed previously, the upper bound for the energy margin in Fig. 2. We stress again that this is true only if the condition on the transverse conductance, Eq. (14) is satisfied. A striking counter-example was given by the DPC-U coils already mentioned above, wound using a CICC with formvar insulated strands [14]. Owing to the very low interstrand conductance the current transfer time was extremely long (up to several hours), so that the energy generated by the Joule heating of a single strand was sufficient to eventually quench the whole cable.

So far we have examined the effect of current distribution from a *collective* point of view, i.e. in terms of the overall cable energy margin against a uniform energy input in the cable cross section. However, collective behaviour is not the only aspect to be considered in a cable with non-uniform current distribution, especially when dealing with pulsed magnets. The current distribution function α can change in time, for instance during a ramp of the operating current. In this case we expect both the average value i_{op} and the width i_{max}-i_{op} to vary. Eventually a single strand can hit the critical surface or reach conditions where its energy margin is so small that the natural perturbation spectrum induces a localised transition. A behaviour of this type was shown by the US-DPC solenoid, that demonstrated an unexpected ramp-rate limitation when operated above the limiting current [15]. Based on these results, on dedicated

subsize experiments and on a much simplified model[16], Takayasu showed that cables operated in average below their limiting current do not suffer from severe ramp-rate limitation.

In summary, we can conclude that a CICC should be designed below the limiting current (Eqs. (5) or (9)), taking care that the interstrand resistance is sufficiently small (Eq. (14)) to guarantee fast current distribution. Provided that these two conditions are satisfied, we expect that the full cable heat sink is used for stabilization.

2.4 Hybrid CICC's

For large scale applications the stabilizer fraction needed for protection can be larger than the one necessary for stability. A cost-attractive alternative to the use of high stabilizer to superconductor ratio is then the use of co-wound stabilizer strands. In this case an *hybrid cable* CICC is obtained. For such a configuration we can ask ourselves how much the extra strands will contribute to stability, and in particular in the balance of power generation and removal. This issue, depending in principle on the current redistribution length and times discussed in the previous section, can have a significant cost impact on magnet construction.

Experiments performed by Miller [9] using a resistive heater in a small size CICC have shown that additional copper strands are not efficient in the initial current sharing to decrease the Joule heating and thus displace the power balance. The limiting current for the cables tested agreed with the value obtained taking the copper cross section in the strand only, and ignoring the co-wound strands. Nozawa et al. [16a] performed similar experiments subjecting two small size (12 strands) CICC's with and without copper strands to large field variations (2 T in approximately 10 ms). Their results cannot be considered as conclusive, because the cables had different critical currents owing to the fact that superconducting strands were replaced by pure copper wires. In addition both cables showed excellent stability thus restricting stability transients to a narrow range close to the critical current. In spite of these *caveats*, plotting their results as a function of the operating density in the superconducting strands, and assuming that the energy deposited in the cable must be proportional to the square of the field variation, shows that the presence of additional copper strands has no significant effect on the energy margin.

In the light of these results it seems obvious that co-wound stabilizer strands should be neglected for stability design. An intuitive justification was suggested by Miller [9]. He remarked that the balance recovery condition between heat generation and removal must be fullfilled at the limiting current as soon as the strand is normal and thus carrying the full current. A delay, as would be needed to transfer the current to co-wound stabilizer strands, would cause additional heat and thus perturb irreversibly the delicate heat balance, pushing the transient towards a quench. This qualitative explanation is based on a limited experimental database, and lacks a sound demonstration. Although the neglect of segregated stabilizer strands is a conservative choice, the potential for cost saving does justify further experimental and modelling efforts

2.5 CICC with additional cooling channel

CICC's are known to have a large impedance to the helium flow, a property related to their large wetted perimeter and indeed beneficial for stability. This has however a detrimental

effect on the pressure drop necessary to circulate the helium. This limitation can be overcome by the addition of a cooling channel with a large diameter compared to the hydraulic diameter of the cable itself. This low impedance cooling channel can be delimited by a physical wall [15,17,18], or simply be a space left in the cable [19]. As for co-wound stabilizer strands, we ask ourselves whether this additional helium volume contributes significantly to the cable heat sink. Few available experimental data [20] seem to indicate that when the channel is delimited by a physical wall with small perforation its effect on stability is negligible.

The question of the effect on stability produced by a cooling channel with large perforation is so far unresolved. In principle we must expect effects both on the heat sink and on the heat transfer coefficient. This last is caused mainly by the split of the induced flow between channels, tending to decrease the heat transfer in the cable bundle, and by local transverse flow patterns, tending instead to increase heat transfer. Simulations were performed in the case of large perforation, taking into account the split of the flow but neglecting heat transfer modifications that could be caused by transverse flow[20a]. The results confirm that in the case of large perforation the energy margin of a cable with a separate cooling channel is systematically lower than the value that would be obtained distributing the same helium amount uniformly in the cable space. Furthermore, they show that conservative results are found neglecting the additional cooling channel. It seems therefore appropriate in the design phase to neglect the additional cooling channels in the accounting of the heat sink.

2.6 Operation in superfluid helium

Superfluid helium has been proposed as a cooling alternative in CICC to avoid forced-flow cooling and thus also circunvent the problem of the large hydraulic impedance of the cable. In addition superfluid helium has exceedingly high heat transfer characteristics, compared to normal helium, and therefore has the potential for operation at higher current density still satisfying the heat removal conditions expressed by Eq. (5) or Eq. (9). In fact the physics of heat transfer in superfluid helium is rather involved [21] resulting in a peculiar behaviour of stability. In simplified terms a CICC operated in superfluid helium exhibits a *second* well cooled regime after the first drop located at the limiting current. In this regime the helium is capable of absorbing heat remaining in the superfluid state, i.e. below the transition temperature T_λ. Therefore the stability margin in the second well-cooled regime is given by the heat sink between operation T_{op} and T_λ, and can be significant, up to 200 to 300 kJ/m^3 of helium volume. This heat sink is available as long as the heat flux removed from the strands during Joule heating q_J'' is well below a critical limit q_*'', determined by the superfluid heat transport properties and the geometry of the cable and surrounding helium:

$$q_J'' << q_*'' \tag{15}.$$

An empirical design criterion, developed by Dresner [22], gives an estimate of the maximum heat flux that can be supported by the superfluid helium. For design purposes it is useful to simplify and rearrange the terms in the original expression, so to obtain the following limiting value for the operating current density:

$$J_{op} \approx \sqrt{\frac{K^{1/3}\left(T_\lambda - T_{op}\right)^{1/3}}{\rho_{stab}} \left(\frac{K_p}{d}\right)^{4/3} \frac{f_{stab}\left(f_{SC}+f_{stab}\right)^{4/3}}{f_{he}^{1/3}}} \tag{16}$$

below which the cable operates in the second well-cooled regime.

3. Quench propagation and protection

The study of the protection of a CICC in case of quench involves mainly the following three items:

- maximum (hot-spot) temperature, which should be below a value T_{max} to limit thermal stresses in the coil;
- maximum pressure, which is bounded to a value p_{max} to limit mechanical stresses on the conduit;
- maximum induced outflow, to be used to size venting lines.

In addition the initial propagation of the quench, mostly the voltage growth rate, is of interest to decide on the appropriate detection scheme, sensitivity, threshold and delay.

The power generated by Joule heat, and thus, in last analysis, the amount of stabilizer, is the main parameter determining quench behaviour. Note that because of the large times involved in quench propagation and current dump, the issue of current distribution in the cable does not play a role. For this reason we assume that the complete stabilizer cross section is effective in the transient, including co-wound stabilizer strands in hybrid cables.

Finally, quench propagation in CICC's operated in superfluid helium is a field where both experimental data and theory are lacking. Simulations suggest that the influence of superfluid heat transport on quench propagation is negligible, mainly because the quench front is at a temperature well above the superfluid transition T_λ. In this section we choose simplistically to neglect operation in superfluid helium.

3.1 Hot-spot temperature

The hot-spot temperature in a CICC is determined by the local heat balance of heat generation and heat capacity, and only marginally affected by heat transport in the winding pack. It is therefore possible to predict accurately the maximum temperature without a detailed knowledge of the quench propagation. We write the local adiabatic heat balance as follows:

$$\frac{dT}{dt} = \frac{1}{f_{stab}\gamma(T)} J_{op}^2 \tag{17}$$

where $\gamma(T)$ is a function of the material fractions in the cable and of their temperature dependent volumetric heat capacity and resistivity:

$$\gamma(T) = \frac{\sum_i f_i C_i}{\rho_{stab}} \tag{18}$$

with the index *i* running over all components in the cable. Once the geometry of the cable is given, the function γ only depends on the temperature *T*. In Eq. (17) the actual size of the cable disappears, and it is customary to write the following *universal* expression for the maximum cable space current density corresponding to the specified maximum temperature:

$$\int_{T_0}^{T_{\max}} \gamma(T)dT = \Gamma\left(T_0, T_{\max}\right) = \frac{1}{f_{stab}} \int_0^{\infty} J_{op}^2 dt \tag{19}$$

which provides an immediate design criterion when the behaviour of current is known as a function of time. We can specialize Eq. (19) for the ideal case of constant current before the quench detection time τ_{det}, followed by an exponential dump with time constant τ_{dump}:

$$J_{op} = \sqrt{f_{stab} \frac{\Gamma\left(T_0, T_{\max}\right)}{\left(\tau_{\det} + \frac{\tau_{dump}}{2}\right)}} \tag{20}$$

where the integral of the current decay is equivalent to a constant current transient with an effective duration:

$$\tau_q = \tau_{\det} + \frac{\tau_{dump}}{2} .$$

Two aspects need some care in the heat balance, namely the effect of helium and of structural components. In the definition of the function Γ we have implicitly assumed that all components included have the same temperature. Although this is true for the strands, it is not the case for either helium or conduit. Significant temperature gradients can develop in the cable cross section, which make the definition of Γ inaccurate. Luckily the effect of helium is only marginal (typically of the order of 10 %), both as a consequence of the helium expulsion out of the normal zone and because the heat capacity of strands and structures becomes largely dominant at increasing temperature. On the other hand the conduit can have a significant impact, typically up to a factor 2 in the total heat capacity. A safe choice is to neglect the conduit in the heat balance, with the consciousness that the results will be conservative. At present only direct simulation gives insight on the effect of the temperature gradients in the cable cross section.

3.2 Helium driven quench propagation and the q-l diagram

Miller et al. investigated pressure rise in CICC's and gave expressions for the maximum pressure after a sudden and complete coil quench [23]. The maximum pressure can be written using the material fractions in the cable as:

$$p_{\max} \approx 0.65 f^{0.36} \left(\frac{\left(\frac{L}{2}\right)^3 K_p}{d} \frac{f_{stab} + f_{SC}}{f_{stab}^2 f_{he}^3} \rho_{stab}^2 J_{op}^4 \right)^{0.36} \tag{21}$$

which is used to derive the maximum allowable cable space current density for a specified pressure increase and cable layout [4]. This expression agrees well with experiments reproducing this limiting case, but has been found to largely overestimate the values to be found in practice. The reason is that pressure increase, as well as helium expulsion, is a process strictly determined by the characteristics of quench propagation. The assumption of sudden and complete coil quench, implying instantaneous propagation, is rather unrealistic and seldom found in reality. As recognized by Dresner [24], the main quench propagation mechanism in CICC is hot helium expulsion. The helium in the initial normal zone is heated by the cable, its temperature rises and it expands in the (still) superconducting region driving it into the normal state through convection heat exchange. Dresner postulated that

"*...the velocity of normal zone propagation equals the local velocity of expansion of the helium*"[24].

The result of this approximation is that

"*...the normal zone engulfs no new helium, or in other words that the heated helium comprises only the atoms originally present in the initial normal zone. We are thus led to the picture of a bubble of hot helium expanding against confinement by the cold helium on either side of it*"[25]

This statement has been the basis for the largest part of the analytical work on quench propagation in CICC's.

At present the most complete model of a quenching CICC is the one that has been developed by Shajii and Freidberg [26] who have derived approximate expressions for quench propagation speed and pressure increase based on the neglect of inertia in the equation of helium motion, taking perfect gas properties for the helium, assuming that the cable has a perfect thermal coupling to the helium (i.e. equal temperature in helium and cable) and constant current throughout the transient. They differentiated among four regimes of quench, depending on the quench *strength* (low and high pressure rise regimes), and on the effect of the coil boundary (short and long coil regimes).

Any given quench condition can be located in the appropriate regime using a *universal* diagram derived in [27]. This diagram can be obtained introducing the two following dimensionless variables

$$l = \frac{\lambda L_q}{L} \tag{22}$$

$$q = \frac{L_q J_{op}^{4/3}}{\eta} \tag{23}$$

where the two normalization parameters λ and η are given by:

$$\lambda = 1.7\left(\frac{\rho_0 R T_{\max}}{p_0}\right)\left(\frac{c_0^2 \rho_0}{p_0}\right) \tag{24}$$

$$\eta = \frac{2.6}{R}\left(\frac{p_0^5}{c_0^2\rho_0^5 T_{\max}}\frac{f_{he}}{4K_p f\left(f_{stab}+f_{SC}\right)}f_{stab}^2\gamma_0^2\right)^{\frac{1}{3}} \tag{25}$$

and subscript "0" stands for initial conditions. Once the material fractions are fixed, and the initial conditions of the quench are given the two variables *l* and *q* can be calculated. Depending on their values the quench will evolve in one of the four possible regimes. The boundaries of the four regimes are reported in Tab. 2 from Ref. [22]. Each regime is distinguished by different asymptotic expressions of the propagation velocity and the pressure rise, also given in Tab. 2 in terms of material fractions. These expressions can be used directly to determine the pressure rise and the helium expulsion during a quench. Note that because of the assumptions made in the derivation of the model the perfect gas equation must be used consistently to compute the initial density in Eqs. (24) and (25) and in Tab. 2.

3.3 Quenchback

In recent experiments [28,29], quench propagation in CICC's has been observed to rapidly accelerate from an initial *conventional* phase, with propagation velocity of the order of 1 to 10 m/s, up to velocities exceeding 100 m/s. The reason for the acceleration is the heating of the dense helium column in front of the propagating normal zone through compression and friction work. When the helium temperature reaches the current sharing limit T_{cs}, the strands become resistive and suddenly large lengths of conductor transit to the normal state. The propagation speeds up, with an upper limit set only by the sound speed in helium - a *thermohydraulic quenchback (THQB)* has taken place.

Shajii and Freidberg have extended the quench propagation model discussed in the previous section to the case of THQB [30]. They have introduced a new quantity *M*:

$$M = \frac{1}{\phi_0}\left(\frac{\rho_0 c_0^2}{p_0}\right)\left(\frac{T_{cs}-T_{op}}{T_{op}}\right) \tag{26}$$

useful to identify the region in the *q-l* diagram where a THQB takes place. The quenchback boundaries written as a function of *M* are reported in Tab. 2. A quench initiated within these boundaries will eventually evolve into a THQB before the current dump is finished. Note that no quenchback takes place in the long coil and low pressure rise regime.

THQB onset time and speed have been computed and are given in detail in Ref. [30]. In the most relevant case of long coil and small temperature margin (compared to the initial temperature) their values are given by:

$$t_{qb} = 8.4\left(\frac{f_{he}dc_0^8}{2K_p f\left(f_{stab}+f_{SC}\right)}\right)\left(\frac{1}{RL_q}\frac{f_{stab}\gamma_0}{J_{op}^2}\right)^3\left(\frac{1}{\phi_0}\frac{T_{cs}-T_{op}}{T_{op}}\right)^5 \tag{27}$$

$$v_{qb} = \phi_0\left(\frac{f_{he}d}{2K_p f\left(f_{stab}+f_{SC}\right)\rho_0}\right)^{\frac{1}{3}}\left(\frac{\rho_{stab}J_{CS}^2}{f_{stab}f_{he}}\right)^{\frac{1}{3}}\left(\frac{T_{op}}{T_{cs}-T_{op}}\right)^{\frac{2}{3}} \tag{28}.$$

We notice the extreme sensitivity of THQB onset time t_{qb} with respect to the temperature margin, a fifth power in Eq. (27). This means that small random uncertainties (in the cable design or manufacturing) will produce a large scattering in the quench evolution, a fact that has been already evidenced in simulations and experiments.

A quenchback has beneficial effects on quench detection and on the spread of the energy in the coil, as it causes an acceleration of quench propagation. Nonetheless when considering temperature and voltage evolution for design purposes it is safer to neglect THQB because its onset is bound to a large uncertainty. On the other hand a quench evolving into a THQB will cause a larger pressure increase than in a normal case, of the order of the maximum pressure estimate provided by Eq. (21). It is therefore safer to take THQB into account when designing for pressure rise.

3.4 Cable conduction at the normal front

In the previous sections we have assumed that the helium expansion, with its complexity, is the only mechanism causing quench propagation. In doing this we have stated that the heat flux along the cable length, responsible for the quench propagation, is exclusively due to helium convection. In reality CICC's often need a large amount of stabilizer to provide stability and protection. The stabilizer has good thermal conductivity, hence it can provide a significant contribution to the heat flux at the quench front by means of thermal conduction. This can be a significant effect for short initial normal zones, where the propagation through conduction can indeed be the dominating mode until the normal length becomes sufficiently large to drive a strong helium flow [31]. The effect of conduction can be evaluated, in first approximation, as a *front advance*, i.e. an additional speed of the normal front with respect to the expanding helium bubble. The front advance is given by [31]:

$$v_{ad} = \sqrt{\frac{J_{op}^2}{\gamma_0^2}\frac{K_{stab}}{\rho_{stab}}\frac{1}{T_{cs}-T_{op}}} \tag{29}$$

and modifies, as an additional term, the propagation speed expressions reported in Tab. 2. Note that this correction is only approximate, as it does not take into account the fact that owing to the front advance the helium mass in the expanding bubble is no longer constant. It can be shown that this phenomenon leads to a further acceleration of the quench front which we neglect here.

3.5 Normal voltage

A final parameter of interest for the design of the protection system of a CICC based coil is the voltage in the normal zone. As CICC are mainly used in large scale applications, the coil discharge relies on an external resistor which dominates the voltage drop during dump. Therefore the maximum voltage is usually attained at the coil terminals and is known from the characteristics of the discharge system. Here the main concern is rather on the detection of the quench through a measurement of the normal voltage in the coil operating in a system that can be pulsed or subject to large electromagnetic perturbation. For this purpose we can give here an estimate of the normal voltage development based on the results of the previous sections.

From the expressions presented till now it is easy to verify that for a typical CICC both the temperature growth rate (see Eq. (17)) and the quench velocity (see Tab. 2) are approximately constant or weakly dependent on time. The consequence is that a quench initiating over a length L_q will develop an approximately piecewise linear temperature profile. The temperature is flat in the initial quenched length and linearly decreasing over the remaining length. The total normal length at a time t after the quench initiation will be approximately L_q+2v_qt, a situation schematically depicted in Fig. 3.

The voltage drop $V(t)$ (a function of time) can be found integrating the electric field along the length of this zone, or:

$$V(t) = \frac{J_{op}}{f_{stab}} \int \rho_{stab}\left(T(x,t)\right) dx$$

In general the above integral requires the detailed knowledge of the temperature as a function of space and time. If we take the linear temperature profile of Fig. 3, with maximum temperature T_m in the initial quenched length and temperature T_{op} in the superconducting region, we can approximate the voltage as follows:

$$V(t) \approx \frac{J_{op}}{f_{stab}} \rho_{stab}\left(T_m\right)\left[L_q + \Omega\left(T_m\right) 2v_q t\right] \tag{30}$$

where, according to Eq. (17), the central temperature T_m is approximately given by:

$$T_m(t) \approx T_{op} + \frac{J_{op}^2}{f_{stab}\gamma_0} t \tag{31}$$

and the function $\Omega(T_m)$ gives a measure of the weight of the new normal length $2\ v_q\ t$ compared to the initial length L_q, taking into account the differences in the cable temperature and its distribution. The definition of Ω and a suitable approximation for copper are:

$$\Omega\left(T_m\right) = \frac{\int_{T_{op}}^{T_m} \rho_{stab}(T)dT}{\rho_{stab}\left(T_m\right)\left(T_m - T_{op}\right)} \approx 1 - 0.3\left[1 + \frac{T_m - 47}{\sqrt{289 + \left(T_m - 47\right)^2}}\right] \tag{32}$$

Equations (31) and (32) can be substituted into Eq. (30) providing the explicit relation for the voltage as a function of time that can be used to estimate the initial development of normal voltage once the quench velocity has been computed from Tab. 2 and the correction for cable condution.

3.7 Parallel cooling channel

As mentioned earlier in the discussion on stability, cables with additional cooling channel offer a better steady state flow characteristic because of their reduced hydraulic impedance. This effect is remarkable also during quench, because the low-impedance cooling channel acts as a preferential relief line. We can take into account this effect using the homogenised hydraulic properties of the channels. Assuming that the flow is incompressible, it can be shown that the parallel of two channels (subscripts "1" and "2") is equivalent to a single channel(subscript "eff") with the same total area (i.e. cable space fraction):

$$f_{he,eff} = f_{he,1} + f_{he,2} \tag{33}$$

and an effective friction factor:

$$\frac{1}{\sqrt{f_{eff}}} \approx \sqrt{\frac{K_p}{d}\frac{f_{stab}+f_{SC}}{f_{he}}}\left(\frac{f_{he,1}}{f_{he,eff}}\sqrt{\frac{D_h}{f}}\bigg|_1 + \frac{f_{he,2}}{f_{he,eff}}\sqrt{\frac{D_h}{f}}\bigg|_2\right) \tag{34}.$$

The two expressions above allow to adapt the equations given so far for quench propagation to the case of a CICC with cooling channel.

4. An example of cable optimization

As an example of application of the equations collected in this paper, we have performed an optimisation of the stabilizer fraction in the case of a Nb_3Sn CICC at 12 and 13 T maximum field. The main parameters chosen for this case study are reported in Tab. 3. A strand diameter of 0.8 mm was chosen, and an upper limit of 2.5 was assumed for the copper:non-copper ratio. Finally, the cable design was performed for a void (helium) fraction of 40 %. The copper fraction was scanned from the minimum to the maximum possible values (i.e. 0 to 0.6), computing for each value of the copper and superconductor fractions the maximum allowed current density defined by Eq. (5) for the limiting current, Eq. (9) for the lower limiting current and Eq. (20) for the maximum hot-spot temperature. All curves are increasing functions of the copper fraction until the limit on the copper:non-copper ratio is reached. Note the slope change for the limiting current density and lower limiting current density at the maximum copper:non-copper ratio, due to the fact that above this limit any additional copper fraction cannot be used for stabilization. Equation (2) was used to calculate the current sharing temperature that gives the requested heat sink, namely 500 mJ/cm^3 as given in Tab. 3. This corresponds to a current sharing temperature of $T_{cs} \approx 5.5$ K, that is a temperature margin of approximately 1 K. The cable space current density corresponding to this temperature margin is proportional to the superconductor fraction, and is plotted as a solid line in Fig. 4. Finally, because of the non-linearity of the quench equations reported in Tab. 2, the maximum pressure limit calculation requires some approximation. The procedure followed here was to use the expressions in Tab. 2 to compute the quench regime, quench velocity and pressure corresponding to the current density at the maximum temperature (hot-spot) limit. It was found that for the conditions used here the quench would develop in the short coil, low pressure rise regime. The ratio of the quench pressure computed in this way to the maximum allowable specified p_{max} was then used to extrapolate the current density to the maximum pressure current density limit, based on the power scaling laws also reported in Tab. 2. Note

that this is only an approximation, because a change of cable space current density could result in a change of quench regime.

The results of the scans are reported in Fig.4. At a field of 12 T the best selection of copper fraction is found at 43 % of the cable space, right at the maximum allowable copper:non-copper ratio of 2.5. The optimal cable space current density is approximately 65 A/mm^2, and the cable is limited by protection (maximum temperature limit). At a higher field of 13 T the temperature margin limit decreases considerably, while the other limits are practically unchanged. This shifts the optimal intersection towards lower copper content. The optimal copper fraction at 13 T is around 36 %, for a copper:non-copper ratio of 1.5, and the maximum cable space current density is 62 A/mm^2. Note that in this particular condition the copper fraction needed for stability is identical to the one needed for protection, resulting in the best possible use of the stabilizer.

5. Conclusions

This paper collects formulae for CICC design, as they have been developed during the last 20 years, bringing them into a uniform notation. It includes, as far as possible, the evolution of the understanding of CICC stability and protection, and addresses new features of CICC layout (cooling channel, hybrid cables) and operation (superfluid helium). The formulae presented here can be used as a platform for a cost-based optimization at guaranteed stability and protection performance. With respect to earlier work, the improved knowledge allows to decrease safety margins and to predict better the actual cable behaviour. Open questions remain mainly in the field of synergistic interaction of cable current distribution and stability. Here both analytical and experimental work is requested before valid design criteria can be proposed and confirmed.

Acknowledgments

All equations reported here have been programmed by Dr. C. Rosso of CryoSoft in a FORTRAN program that has been used for the sample optimizations presented.

References

[1] L. Dresner, *Twenty years of Cable-in-Conduit Conductors*, J. Fus. En., **14**, 1, 3-12, 1995

[2] J.R. Miller, *The Development of Force-Cooled Superconductors for use in Large Magnets*, Adv. Cryo. Eng., **27**, 207-216, 1982.

[3] L. Dresner, *Rational Design of High-current Cable-in-Conduit Superconductors*, IAEA-TECDOC-594, 149-163, 1991.

[4] L. Bottura, *Stability, Protection and AC Loss of Cable-in-Conduit Conductors. A Designer's Approach*, Fusion Engineering and Design, **20**, 351-362, 1992.

[5] L. Dresner, *Parametric Study of the Stability Margin of Cable-in-Conduit Superconductors: Theory*, IEEE Trans. Mag., **17**, 1, 753, 1981.

[6] J.H. Schultz, J.V. Minervini, *Sensitivity of Energy Margin and Cost Figures of Internally Cooled Cabled Superconductors (ICCS) to Parametric Variations in Conductor Design*, Proc. 9th Magn. Tech. Conf., Zurich , 643-646, 1985.

[7] C. Schmidt, *Stability of Superconductors in Rapidly Changing Magnetic Fields*, Cryogenics, **30**, 501, 1990.

[8] Z.J.J. Stekly, J.L. Zar, *Stable Superconducting Coils*, Tans. Nucl. Sci., 367, 1965.

[9] J.R. Miller, *Empirical Investigation of Factors Affecting the Stability of Cable-in-Conduit Superconductors*, Cryogenic, **25**, 552-557, 1985.

[10] W. Lue, *Review of Stability Experiments on Cable-in-Conduit Conductors*, Cryogenics, **34**, 10, 779-786, 1994.

[11] L. Bottura, *Limiting Current and Stability of Cable-in-Conduit Conductors*, Cryogenics, **34**, 10, 787-794, 1994.

[11a] Y. Takahashi, et al., *Experimental Results of Stability and Current Sharing of NbTi Cable-in-Conduit Conductors for the Poloidal Field Coils*, IEEE Trans. Appl. Sup., **3**, 1, 610-613, 1993.

[12] G. Ries, *Stability in Superconducting Multistrand Cables*, Cryogenics, **20**, 513-519, 1980.

[13] M. Takayasu, *Strand Contact Resistance*, private communication, 1992.

[14] N. Koizumi, et al., *Experimental Results on Instability Caused by Non-Uniform Current Distribution in the 30 kA NbTi Demo Poloidal Coil (DPC-U) Conductor*, Cryogenics, **34**, 2, 155-162, 1994.

[15] M.M. Steeves, et al., *Test Results from the Nb3Sn US-Demonstration Poloidal Coil*, Adv. Cryo. Eng., **37**, A, 345-354, 1991.

[16] M. Takayasu, et al., *Measurements of Ramp-rate Limitation of Cable-in-Conduit Conductors*, IEEE Trans. Appl. Sup., **3**, 1, 456-459, 1993.

[16a] M. Nozawa, et al., *Experimental Investigation of Stability in Cable-in-Conduit Conductors Subjected to Varying Field due to Plasma Disruption*, Adv. Cryo. Eng., **42**, 1265-1271, 1996.

[17] S. Foerster, U. Jeske, A. Nyilas, *Fabrication of a 15 kA NbTi-Cable for the 150 T/s High Ramp Rate POLO Model Coil*, Proc. 15th SOFT, Utrecht, The Netherlands, 1557-1564, 1989.

[18] D.L. Walker, F.M. Kimball, E.R. Kimmy, R.J. Loyd, S.D. Peck, H.H. van der Bergh, *Design of a 200 kA Conductor for Superconducting Magnetic Energy Storage (SMES)*, Adv. Cryo. Eng., **35**, A, 573-579, 1990.

[19] C.C. Baker, B. Montgomery, K.L. Wilson, *ITER - A World Class Challenge Opportunity*, IEEE Trans. Appl. Sup., **5**, 2, 61-68, 1995.

[20] C.A. Luongo, K.D. Partain, J.R. Miller, G.E. Miller, M. Heiberger, A. Langhorn, *Quench initiation and propagation study (QUIPS) for the SMES-CICC*, Cryogenics, **34**, 611-614, 1994

[20a] S. De Palo, C. Marinucci, R. Zanino, *Stability Estimates for CICC's with Cooling Channels Using 1- and 2-Fluid Codes*, to appear in Adv. Cryo. Eng., 1998.

[21] S. van Sciver, *Helium Cryogenics*, Clarendon Press, 1986.

[22] L. Dresner, *A Rapid, Semiempirical Method of Calculating the Stability Margins of Superconductors Cooled with Subcooled He-II*, IEEE Trans. Mag., **23**, 2, 918-921, 1987.

[23] J.R.Miller, L.Dresner, J.W.Lue, S.S.Shen, H.T.Yeh, Pressure Rise during the Quench of a Superconducting Magnet Using Internally Cooled Conductors, Proc. of ICEC-8, Genova, 1980, 321-329

[24] L.Dresner, The Growth of Normal Zones in Cable-in-Conduit Superconductors, Proc. of 10th Symp on Fusion En., 1983, 2040-2043

[25] L.Dresner, Protection Considerations for Force-Cooled Superconductors, Proc. of 11th Symp on Fusion En., 1985, 1218-1222

[26] A.Shajii, J.P.Freidberg, Quench in Superconducting Magnets. II. Analytic Solution, J. Appl. Phys., **76**, (5), 1994, 3159-3171

[27] A.Shajii, J.P.Freidberg, E.A.Chaniotakis, Universal Scaling Laws for Quench and Thermal Hydraulic Quenchback in CICC Coils, IEEE Trans. Appl. Superconductivity, **5**, (2), 1995, 477-482

[28] J.W.Lue, et al., *Investigating Thermal Hydraulic Quenchback in a Cable-in-Conduit Superconductor*, IEEE Trans. Appl. Superconductivity, **3**, 338-341,1993.

[29] T.Ando, et al., *Measurement of Quench Back Behavior on the Normal Zone Propagation Velocity in a CICC*, Cryogenics, **34**, 599-602, 1994.

[30] A.Shajii, J.P.Freidberg, *Theory of Thermal Hydraulic Quenchback*, Int. J. Heat Mass Transfer, **39**, 3, 491-501, 1996.

[31] L. Bottura, *The Influence of Cable Conduction on Quench Propagation in Force-Flow Cooled Conductors*, Supercond. Sci. Technol., **9**, 141-144, 1996.

$A_{CS}=A_{he}+A_{SC}+A_{stab}$	[m^2]	cable space
A_{he} , A_{SC} , A_{stab}	[m^2]	cross sections of helium, superconductor, stabilizer
c	[m/s]	sound speed in helium
C_{he} , C_{SC} , C_{stab}	[J/Km^3]	heat capacity of helium, superconductor, stabilizer
d	[m]	strand diameter
ΔE	[J/m^3]	energy margin
D_h	[m]	hydraulic diameter
ΔT	[K]	temperature margin
f	[-]	friction factor
ϕ	[-]	Gruneisen parameter for helium
f_{he} , f_{SC} , f_{stab}	[-]	fraction of helium, superconductor, stabilizer
γ	[J/Ωm^4K]	hot spot heating rate function
Γ	[J/Ωm^4]	hot spot integral
G'	[Ω^{-1}/m]	interstrand conductance per unit length
h	[W/K m^2]	heat transfer coefficient
η	[$A^{4/3}/m^{5/3}$]	quench strength scaling parameter
I	[A]	current
J	[A/m^2]	current density
K	[W^3/m^5K]	superfluid helium conductivity function
K_p	[-]	wetted perimeter reduction factor
K_{stab}	[W/m K]	stabilizer thermal conductivity
l	[-]	dimensionless quench length variable
λ	[-]	quench length scaling parameter
L , L_q	[m]	coil length, initial quenched length
L',M'	[H/m]	strand self and mutual inductances per unit length
L_i	[m]	current transfer length
M	[-]	dimensionless quenchback parameter
p	[Pa]	pressure
p_w	[m]	wetted perimeter
θ	[rad]	average cabling angle
q	[-]	dimensionless quench strength variable
R	[J/Kg K]	helium gas constant
ρ	[Kg/m^3]	helium density
R'	[Ω/m]	strand resistance per unit length
ρ_{stab}	[W m]	stabilizer resistivity
T	[K]	temperature
τ_e , τ_r , τ_i , τ_{det} , τ_{dump}	[s]	characteristic time of energy deposition, recovery, current transfer, detection, dump
v	[m/s]	velocity
V	[V]	voltage

Table 1. List of symbols

long coil, high pressure rise		short coil, high pressure rise	
regime boundary	quenchback boundary	regime boundary	quenchback boundary
$q > 1$ $q > l^{5/6}$	$q > M^{5/3}$	$q > 1.2\, l^{1/3}$ $q < 1.1\, l^{5/6}$	$q > \frac{l^{1/3}}{2}\left[1+\sqrt{1+4(l-M)}\right]$
$v_q = 0.766\left(\frac{f_{he} d}{2K_p f\left(f_{stab}+f_{SC}\right)\tau_q}\right)^{\frac{1}{5}}\left(\frac{RL_q}{c_0}\frac{J_{op}^2}{f_{stab}\gamma_0}\right)^{\frac{2}{5}} \propto J_{op}^{4/5}$ $\Delta p = \frac{R\rho_0 L_q}{2v_q}\frac{J_{op}^2}{f_{stab}\gamma_0} \propto J_{op}^{6/5}$		$v_q = \left(\frac{f_{he} d}{2K_p f\left(f_{stab}+f_{SC}\right)}\frac{RL_q}{L}\frac{J_{op}^2}{f_{stab}\gamma_0}\right)^{\frac{1}{3}} \propto J_{op}^{2/3}$ $\Delta p = \frac{R\rho_0 L_q}{2v_q}\frac{J_{op}^2}{f_{stab}\gamma_0} \propto J_{op}^{4/3}$	
long coil, low pressure rise		**short coil, low pressure rise**	
regime boundary	quenchback boundary	regime boundary	quenchback boundary
$q < 0.8$ $q > l^{2/3}$	-	$q < 1.2\, l^{1/3}$ $q < l^{2/3}$	$q > M^{1/3}$
$v_q = \frac{R\rho_0 L_q}{2p_0}\frac{J_{op}^2}{f_{stab}\gamma_0} \propto J_{op}^2$ $\Delta p = 1.36\,\rho_0 c_0\left(\frac{2K_p f\left(f_{stab}+f_{SC}\right)\tau_q v_q^3}{f_{he} d}\right)^{\frac{1}{2}} \propto J_{op}^3$		$v_q = \frac{R\rho_0 L_q}{2p_0}\frac{J_{op}^2}{f_{stab}\gamma_0} \propto J_{op}^2$ $\Delta p = \left(\frac{K_p f\left(f_{stab}+f_{SC}\right)\rho_0 L}{f_{he} d}\right)v_q^2 \propto J_{op}^4$	

Table 2. Summary of regime boundaries and relevant expressions for the propagation speed and the pressure rise in the four regimes of helium-driven quench propagation in a CICC. The scaling of quench velocity and pressure increase with the cable space current density is also reported.

operating temperature	T_{op}	[K]	4.5
operating pressure	p	[bar]	5
detection time	τ_{det}	[s]	1
current dump time	τ_{dump}	[s]	15
coil length	L	[m]	300
initial quenched length	L_q	[m]	1
minimum energy margin	ΔE	[mJ/cm^3]	500
maximum quench temperature	T_{max}	[K]	150
maximum quench pressure	p_{max}	[bar]	150

Table 3. Main parameters used for the optimization scans reported in Fig. 4

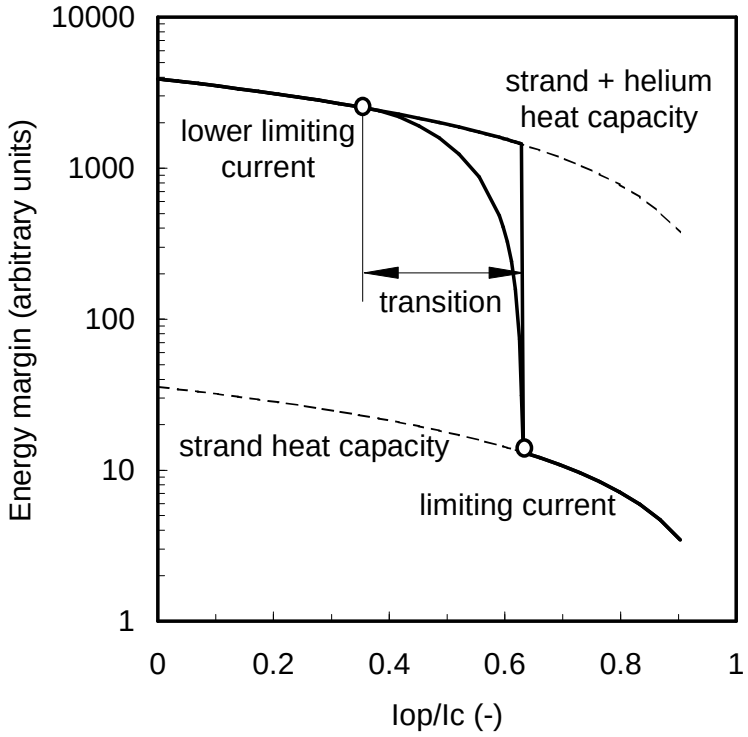

Figure 1. Schematic representation of the stability margin for a CICC with uniform current distribution. The upper and lower dashed lines are the minimum (strands) and maximum (strands + helium) heat sinks. The approximation of the stability margin after the well-cooled/ill-cooled model has a discontinuity located at the limiting current. A more realistic approximation is obtained using the recovery temperature model, with a continuous transition from the upper value at the lower limiting current to the lower value at the limiting current.

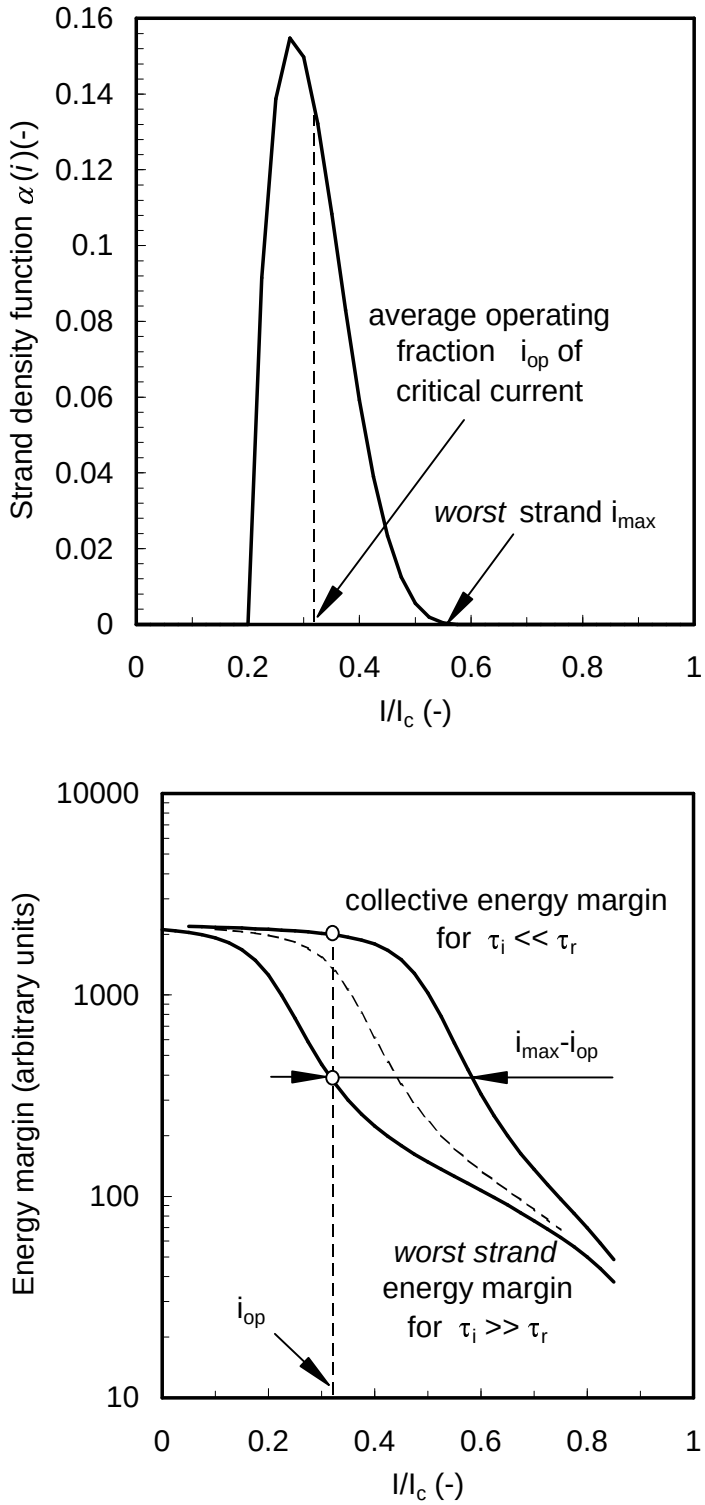

Figure 2. Schematic representation of the effect of non-uniform current distribution on the stability of a CICC. For the arbitrary current distribution function (top) with average value i_{op} and maximum value i_{max} (*worst* strand) the CICC energy margin (bottom, dashed line) has an upper bound given by the energy margin of the cable with uniform current distribution (upper solid line) and a lower bound given by the energy margin of the strand carrying the normalised current i_{max} (lower solid line).

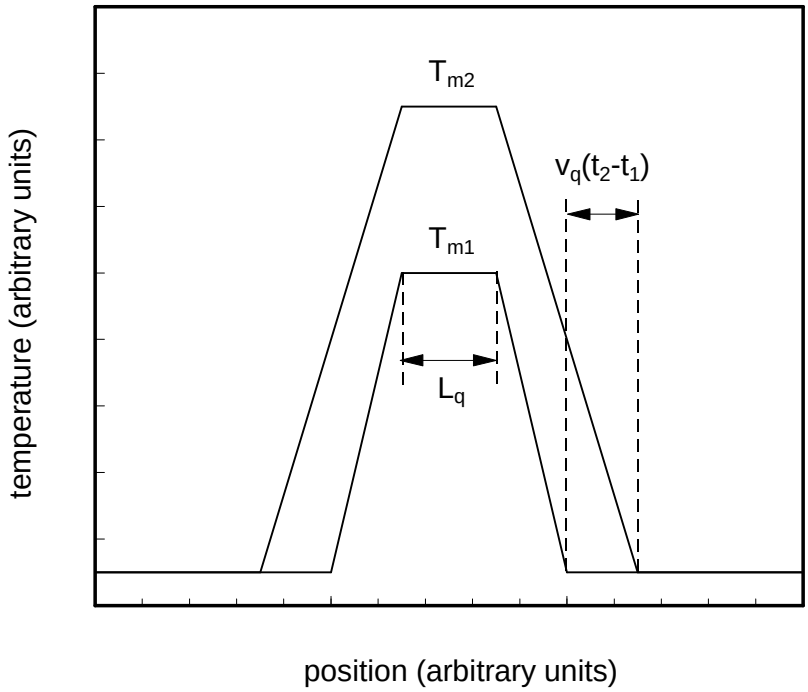

Figure 3. Schematic temperature distribution along a cable at two times (t_1 and t_2) during a quench, used to approximate the initial normal voltage evolution. The initial quenched length L_q is assumed to propagate at constant speed v_q.

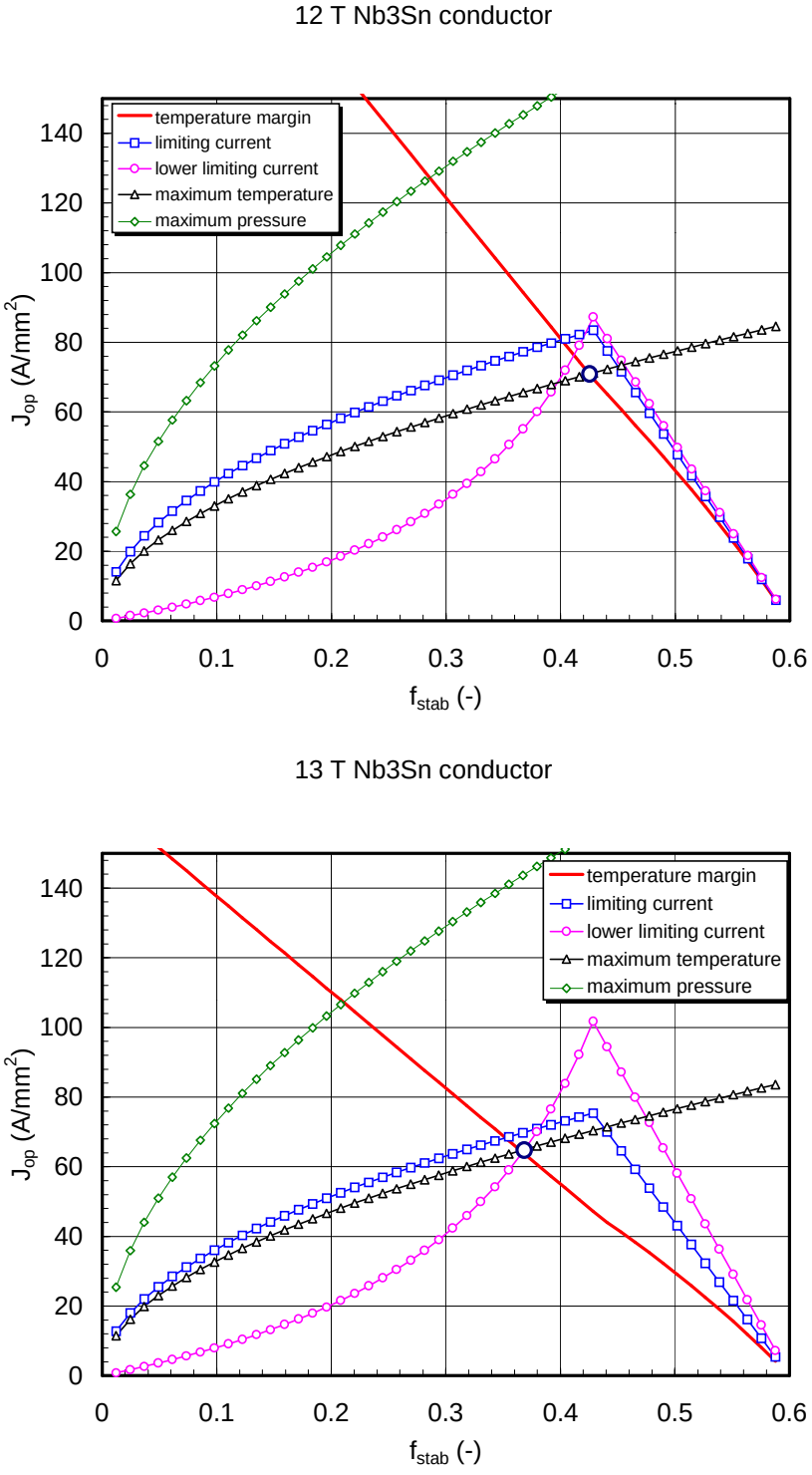

Figure 4. Sample optimizations for a Nb3Sn based CICC at 12 and 13 T, obtained using the procedure described in this paper. The conductor is protection dominated at 12 T, and becomes stability dominated at 13 T. The optimal deisgn point is marked with a circle in the plots.